CDF Note 8588

Search for Single Top Quark Production in 955 pb^{-1} using the Matrix Element Technique

The CDF Collaboration
URL http://www-cdf.fnal.gov
(Dated: November 8, 2006)

We present a search for electroweak single top quark production using 955 pb^{-1} of CDF II data collected between 2002 and 2005. The analysis employes a matrix element technique which is used to calculate event probabilities for the signal and background hypothesis. The ratio of signal and background event probability is used as a discriminant variable which we fit to the data. We search for a combined single top s- and t-channel signal and measure a cross section of $2.7^{+1.5}_{-1.3}$ pb (systematics included) assuming a top quark mass of 175 GeV/c^2. We use the CLs/CLb method to calculate the signal significance. The observed p-value in 955 pb^{-1} of CDF data is 1.0 %. The expected (median) p-value in pseudo-experiments is 0.6%.

Preliminary Results for DPF Hawaii, Nov 2006

INTRODUCTION

The measurement of electroweak single top production probes the W-t-b vertex and provides a direct determination of the Cabbibo-Kobayashi-Maskawa (CKM) matrix element $|V_{tb}|$. This quantity is essentially still unmeasured and all previous results were made under the assumption that the CKM matrix is unitary. A measurement of single top production allows an alternate way to exclude a hypothetical fourth quark generation, and to allow tests of exotic models beyond the Standard Model which predict anomalously altered single top production rates like heavy right handed $W^{\pm}$ bosons, flavor changing neutral currents or large extra dimensions [1].

Finding single top quark production is challenging since it is rarely produced ($\sigma_{singletop}$ ~2.9 pb in the Standard Model [2]) in comparison with other processes with the same final state like W+jets and $t\bar{t}$. The signal to background ratio of the analysis is small, typically on the order of S/B~1/20. This calls for a better discrimination of signal and background events which can be achieved by using more information to characterize each event.

In this analysis, we have employed an analysis technique that attempts to make optimal use of information in the data, the Matrix Element technique. In this method, improved sensitivity is achieved by exploiting matrix element calculations of signal and background probability densities to build a likelihood function. Although the implementation of this method is derived from a precision measurement of the top quark mass and of the W Helicity in $t\bar{t}$ lepton+jets events [3], a novel feature of this analysis is the application of this technique to a search.

DATA SAMPLE & EVENT SELECTION

Candidate events for this analysis are selected by requiring a W + 2 jet event topology where the W decays leptonically, $W \to e\nu_e$ and $W \to \mu\nu_\mu$. One or both of the two jets should be identified as a b-jet using the secondary vertex tag requirement. The secondary vertex tag identifies tracks associated with the jet originating from a vertex displaced from the primary vertex. We further require the missing transverse energy and the jets not to be collinear for low values of missing transverse energy. This requirement removes a large fraction of the non-W background while retaining most of the signal. Our major backgrounds are W + heavy flavor events, which closely mimic s-channel single top production; mistags which are W + light quark events that are mistakenly tagged as b jets; non-W, which are multijet events in which a jet is mistakenly identified as a lepton and another jet mismeasured, providing a false missing transverse energy signature; and top pair production events in which one lepton or two jets are not reconstructed, closely resembling the the kinematics of single top production. Table I lists the expected event yield. and Figure 1 shows the composition of signal and background events as a function of number of bins.

Process	Number of Events in 955 pb^{-1}
s-channel	15.44±2.23
t-channel	22.36±3.64
$Wb\bar{b}$	170.9±50.7
$mistags$	136.1±19.7
$Wc\bar{c}$	63.5±19.9
Wcj	68.6±19.0
$non-W$	26.2±15.9
WW	5.51±0.96
WZ	7.96±0.83
ZZ	0.25±0.06
$Z(\to ee)jj$	1.18±0.45
$Z(\to \mu\mu)jj$	5.25±1.55
$Z(\to \tau\tau)$	5.49±2.42
$t\bar{t}$ dilepton	19.86±4.57
$t\bar{t}$ non-dilepton	38.49±8.89
Total signal	37.80±5.87
Total background	549.3±95.1
Total prediction	587.1±96.5
Observed in data	644

TABLE I: Number of expected single top and background events in 955 pb^{-1} of CDF data passing all event selection requirements.

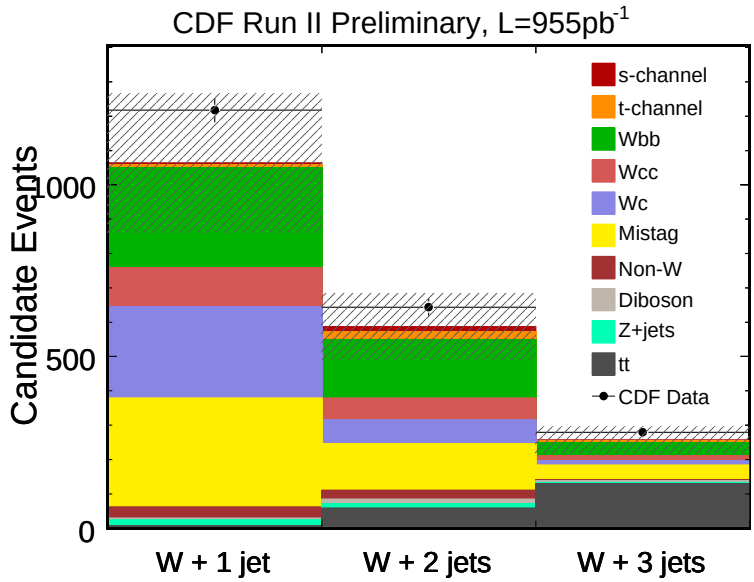

FIG. 1: Number of jets for the expected signal and background event composition. Uncertainties on the data are statistical; the hatch marks represent systematic errors in the background estimate.

METHOD

This analysis is based on a Matrix-Element method in order to maximize the use of information in the events [3]. We calculate event probability densities under the signal and background hypotheses as follows. Given a set of measured variables of each event (the 4-vectors of the lepton and the two jets), we calculate the probability densities that these variables could result from a given underlying interaction (signal and background). The probability density is constructed by integrating over the parton-level differential cross-section $d\sigma$, which includes the matrix element for the process, the parton distribution functions $f(x_i)$, and the detector resolutions parameterized by transfer functions $W(y,x)$:

$$P(x) = \frac{1}{\sigma}\int d\sigma(y) dq_1 dq_2 f(x_1) f(x_2) W(y,x) \tag{1}$$

This analysis calculates probability densities for four different underlying processes: s-channel, t-channel, $Wb\bar{b}$, and Wc + jet. The transfer functions $W(x,y)$ are used to include detector effects. Lepton quantities and jet angles are considered to be well measured. However, jet energies are not, and their resolution is parameterized from Monte Carlo simulation to create a jet resolution transfer function. We integrate over the quark energies and over the z-compoment of the neutrino four momentum to create a final probability density.

We use these probability densities to construct a discriminant variable for each event. The two single-top channels are combined to form a single signal probability density. We also introduce extra non-kinematic information by using the output (b) of a neural network b-tagger which assignes a probability ($0 < b < 1$) for each b-tagged jet of originating from a b quark. The discriminant variable is then constructed as:

$$EPD = \frac{b \cdot P_{singletop}}{b \cdot P_{singletop} + b \cdot P_{Wbb} + (1-b) \cdot P_{Wcc} + (1-b) \cdot P_{Wcj}} \tag{2}$$

We construct a histogram from of our predicted values and shapes for each background. The combined s- and t-channel discriminant for all signal and background processes is shown in Figure 2.

We perform a binned likelihood fit to the data, in which the background shapes are constrained by a Gaussian, but the signal has no constraint. The fit determines the most probable value of the single-top cross section. The likelihood

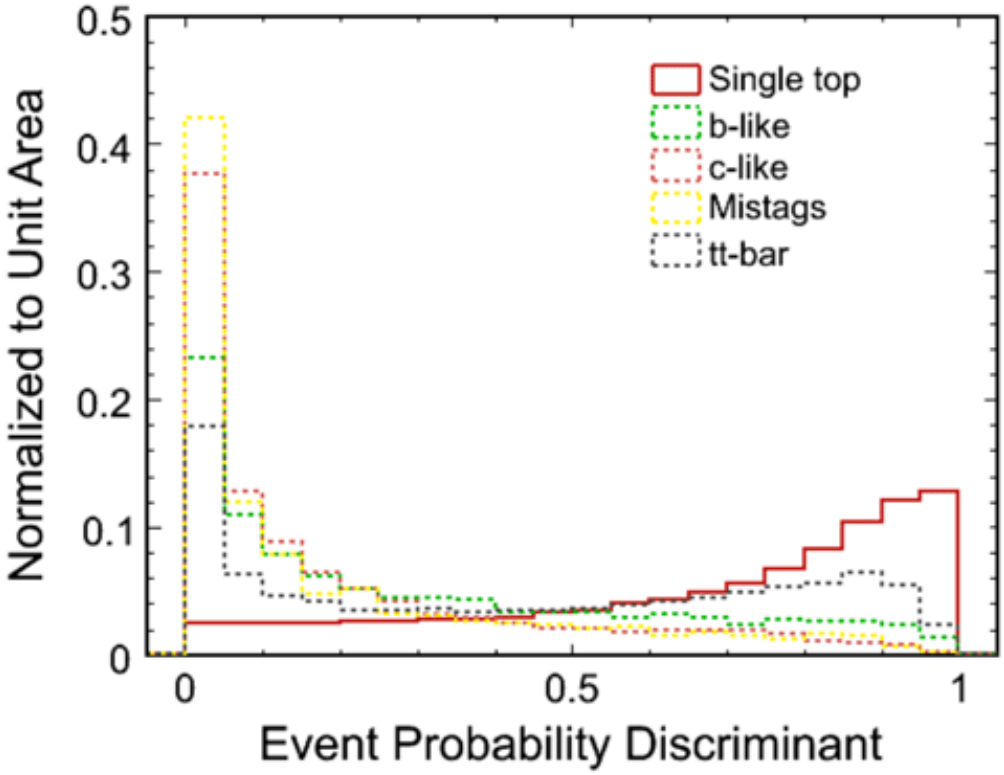

FIG. 2: Combined s-channel and t-channel discriminant for all signal and background processes. All histograms are normalized to unit area.

function includes the systematic uncertainties on the background normalization and other systematic effects, which can affect a sample's normalization, shape, or both.

SYSTEMATIC UNCERTAINTIES

We address systematic uncertainty from several different sources: (1) jet energy scale (2), initial state radiation (ISR) (3), final state radiation (FSR), (4) parton distribution functions, (5) the event generator, the uncertainty in the event detection efficiency and luminosity, (6) Neural Network b-tagger uncertainty, (7) ALPGEN Monte Carlo Factorization/Renormalization scale uncertainty, (8) uncertainty on the mistag model, (9) uncertainty on the non-W model, and (10) uncertainty on the non-W flavor composition. Systematic uncertainties can influence both, the expected event yield (normalization) and the shape of the discriminant distribution.

Normalization uncertainties are estimated by recalculating the acceptance using Monte Carlo samples altered due to a given systematic effect. The single top normalization uncertainty is the difference between the systematically shifted acceptance and the default one and is shown in Table II.

The effect of the uncertainty in the jet energy scale is evaluated by applying jet-energy corrections that describe $\pm 1\sigma$ variations to the default correction factor. Systematic uncertainties due to the modeling of ISR and FSR are obtained from dedicated Monte Carlo samples where the rate of ISR/FSR was increased and decreased in the parton showering to represent $\pm 1\sigma$ variations. To evaluate the uncertainty associated with the specific choice of parton distribution functions, we vary the 40 independent eigenvectors of the CTEQ parton distribution functions and compare to the MRST PDFs. We quadratically sum the uncertainty from the CTEQ and MRST PDF uncertainty.

For all backgrounds the normalization uncertainties are represented by the uncertainty on the predicted number of background events and are incorporated in the analysis as Gaussian constraints $G(\beta_j|1,\Delta_j)$ in the likelihood fit:

$$\mathcal{L}(\beta_1,\ldots,\beta_5;\delta_1,\ldots,\delta_{10}) = \underbrace{\prod_{k=1}^{B}\frac{e^{-\mu_k}\cdot\mu_k^{n_k}}{n_k!}}_{Poisson\ term}\cdot\underbrace{\prod_{j=2}^{5}G(\beta_j|1,\Delta_j)}_{Gauss\ constraints}\cdot\underbrace{\prod_{i=1}^{10}G(\delta_i,0,1)}_{Systematics} \tag{3}$$

$$where,\ \mu_k = \sum_{j=1}^{5}\beta_j\ \cdot\ \underbrace{\left\{\prod_{i=1}^{10}[1+|\delta_i|\cdot(\epsilon_{ji+}H(\delta_i)+\epsilon_{ji-}H(-\delta_i))]\right\}}_{Normalization\ Uncertainty} \tag{4}$$

$$\underbrace{\cdot\ \alpha_{jk}}_{Shape\ P.}\ \cdot\ \underbrace{\left\{\prod_{i=1}^{10}(1+|\delta_i|\cdot(\kappa_{jik+}H(\delta_i)+\kappa_{jik-}H(-\delta_i)))\right\}}_{Shape\ Uncertainty} \tag{5}$$

All systematic normalization and shape uncertainties are incorporated into the likelihood as nuisance parameters, conforming with a fully Bayesian treatment [5]. We take the correlation between normalization and shape uncertainties for a given source into account [6]. The relative strength of a systematic effect due to the source i is parameterized by the nuisance parameter δ_i in the likelihood function, constrained to a unit-width Gaussian (last term in Equation 3). The $\pm1\sigma$ changes in the normalization of process j due to the ith source of systematic uncertainty are denoted by $\epsilon_{ji}+$ and $\epsilon_{ji}-$ (see Equation part 4). The $\pm1\sigma$ changes in bin k of the EPD templates for process j due to the ith source of systematic uncertainty are quantified by κ_{jik+} and κ_{jik-} (see Equation part 5). $H(\delta_i)$ represents the Heaviside function, defined as $H(\delta_i)=1$ for $\delta_i>0$ and $H(\delta_i)=0$ for $\delta_i<0$. The Heaviside function is used to separate positive and negative systematic shifts (for which we have different normalization and shape uncertainties). The variable δ_i appears in both the term for the normalization (Equation 4) and the shape uncertainty (Equation 5), which is how correlations between both effects are taken into account. We profile the likelihood function by maximizing $\mathcal{L}(\beta_1,\beta_2,\beta_3,\beta_4,\beta_5,\delta_1,..\delta_{10})$ with respect to the nuisance parameters $\beta_2,\beta_3,\beta_4,\beta_5,\delta_1,..\delta_{10}$ for many possible values of the single top cross-section β_1 from [0..5]. The resulting profile likelihood $\mathcal{L}(\beta_1)$ is a function of the single top cross-section β_1 only.

We list all contributions to the normalization uncertainty for single top and $t\bar{t}$ in Table II and the systematic acceptance change due to jet energy scale uncertainty of the backgrounds in Table III.

(i) Source	s-channel	t-channel	single top	$t\bar{t}$
(1) JES	-1.4%/+1.3%	-2.4%/+1.8%	-2.0%/1.6%	9.1%/-8.2%
(2) ISR	1.1%/-2.0%	2.6%/ 2.0%	2.0%/ 0.3%	3%
(3) FSR	1.3%/1.4%	3.4%/2.2%	2.6%/1.9%	3%
(4) PDF	1.0%/-0.6%	1.7%/-0.3%	1.4%/-0.4%	2.4%
(5) MC Generator	1%	2%	1.6%	3%
(5) ϵ_{evt}	6.3%	8.1%	7.4%	7.1%
(5) Luminosity	6%	6%	6%	6%
( ) Cross section	N/A	N/A	N/A	19.7%
Total	9.1%	10.6%	10.6%	24.3%
Total (without JES)	N/A	N/A	N/A	22.5%

TABLE II: Systematic uncertainties on expected number of single top and $t\bar{t}$ events.

Source	b-like	c-like	Mistags	$t\bar{t}$
(1) JES	-7.4%/+7.0%	-6.8%/+7.7%	-8.9%/10.1%	9.1%/-8.2%

TABLE III: Relative normalization uncertainty due to jet energy scale uncertainty for each background template used in the likelihood fit.

VALIDATION OF THE METHOD

Many tests of this analysis were done comparing simulated (Monte Carlo) samples to the data. We looked at the input variables to ensure the data matched the Monte Carlo. We constructed the EPD discriminant in the zero-tag W+2 jets side-band data, i.e. we select W+2 jets events according to our nominal event selection and require that both jets are *not* tagged. This event selection is orthogonal to the single top signal region while it still represents a very similar kinematic event topology. Another advantage is that this high statistics sample is dominated by W+ 2 jets events with very little contribution from top (<0.5%). Figure 3 shows data/Monte Carlo comparisons for the measured four-vector components of the lepton and the two jets in this side band.

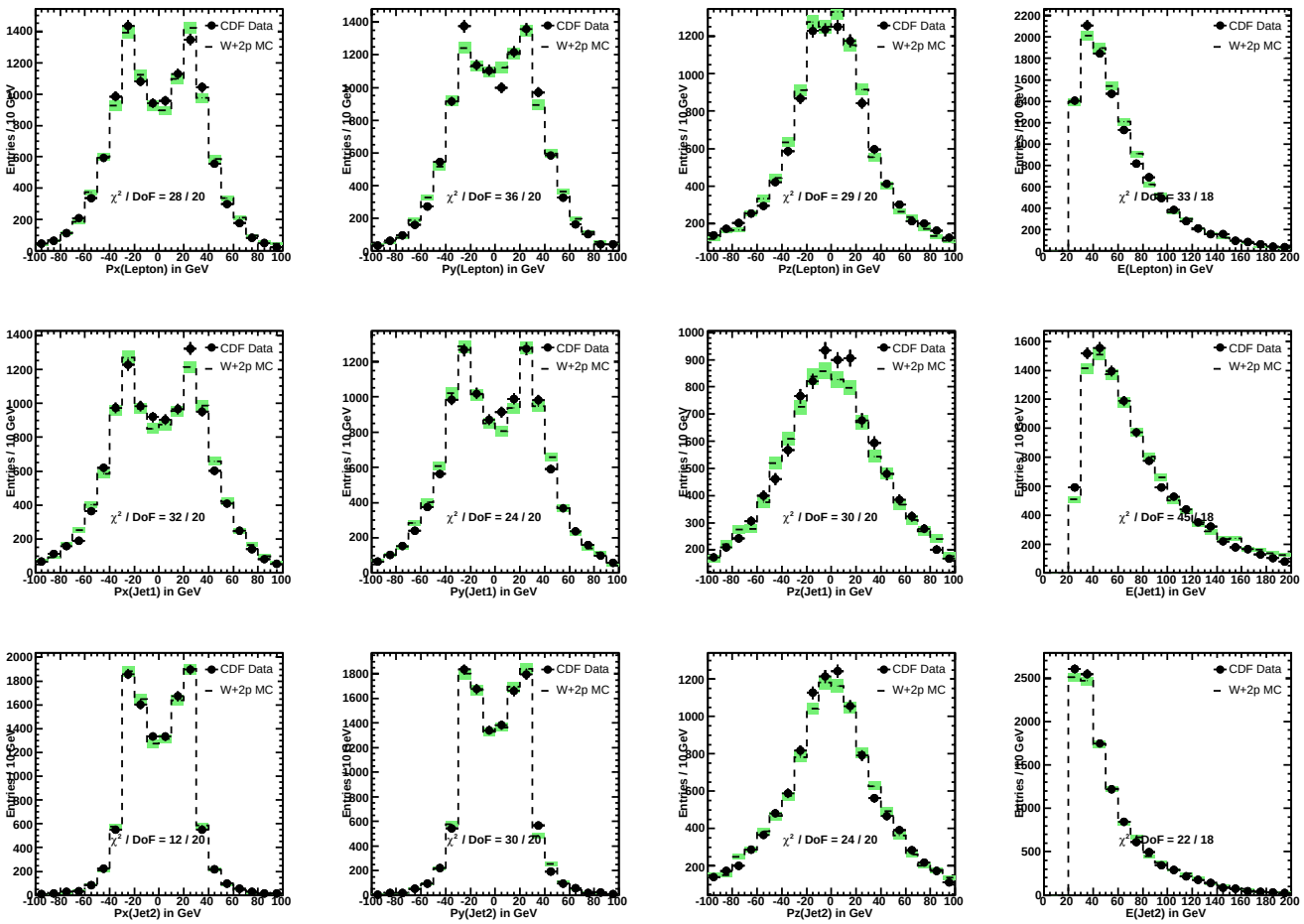

FIG. 3: Comparison of the event probability input 4-vectors for ALPGEN W + 2 jet Monte Carlo and W + 2 jet data in the zero-tagged side band data. The green band accounts for the Monte Carlo statistical uncertainty. The error bars on the data points are Gaussian errors.

We also constructed the discriminant in the dipleton sample (taking only the most energetic lepton) and in the four-jet bin (taking only the two most energetic jets), which should agree well with $t\bar{t}$ Monte Carlo. In all these cases the data and Monte Carlo agreed well.

After performing cross-checks in these data sidebands, we analyze the tagged W+2 jets data, i.e. the single top signal region. Figure 4 shows all six input variables. We compare data to Monte Carlo distributions normalized to the prediction for the tagged W+2 jets data. For shape comparison, the stacked Monte Carlo distributions are scaled to the data using an overall scale factor of 1.1. Within uncertainty, we find good agreement between data and Monte Carlo.

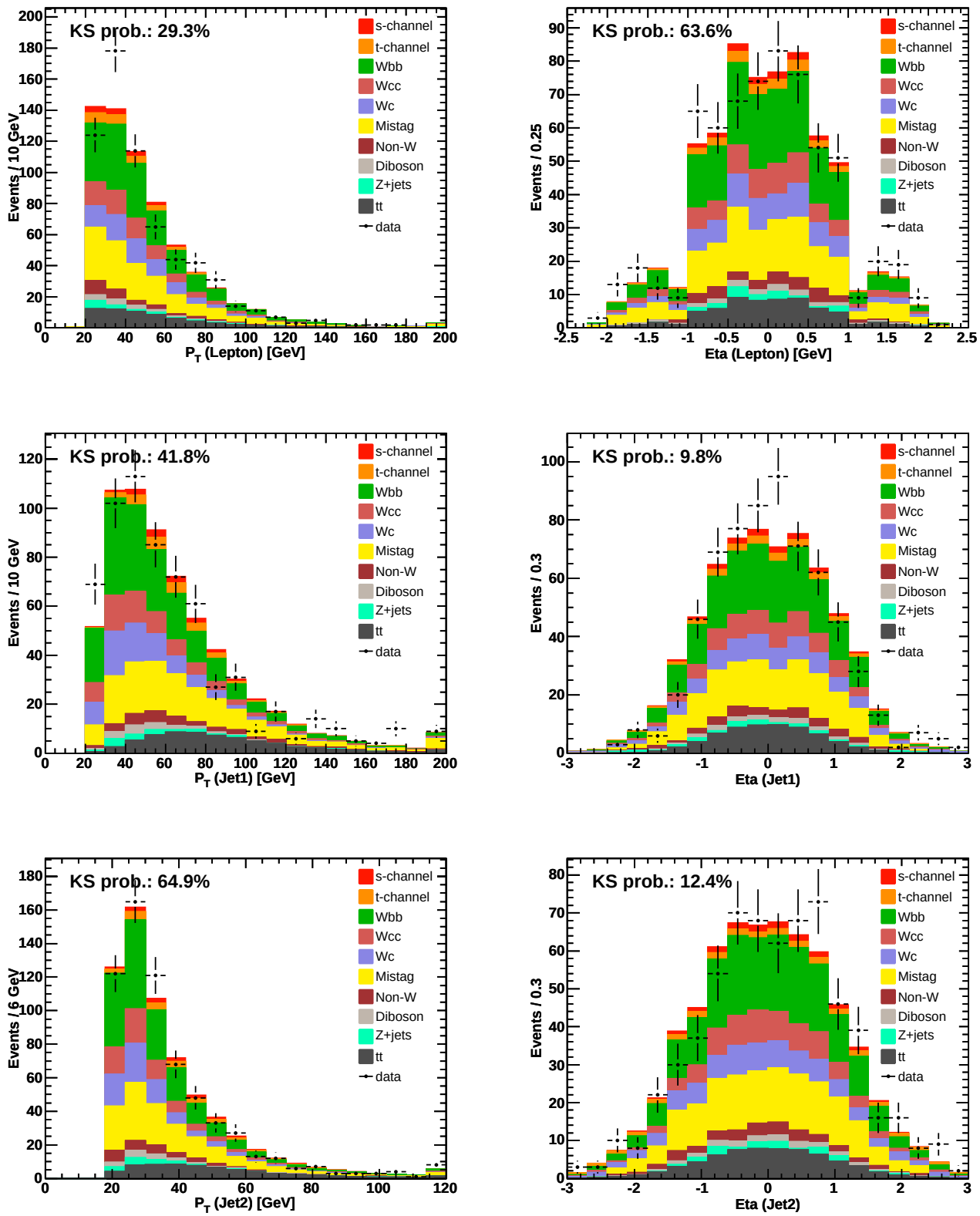

FIG. 4: Comparison of the event probability input variables for Monte Carlo prediction and data in the signal region. For shape comparison, the Monte Carlo prediction is scaled to the data (scale factor=1.096)

RESULTS

We apply the analysis to 955 pb^{-1} of CDF Run II Data. We compare the EPD distribution of 644 candidate events with the sum of predicted single top and background templates as shown in Figure 5 a). In order to extract the most probable single top content in the data we perform a maximum likelihood fit using the method described in the previous section. The posterior p.d.f is obtained by using Bayes' theorem:

$$p(\beta_1|data) = \frac{\mathcal{L}^*(data|\beta_1)\pi(\beta_1)}{\int \mathcal{L}^*(data|\beta_1')\pi(\beta_1')d\beta_1'}$$

where $\mathcal{L}^*(data|\beta_1)$ is the profile likelihood and $\pi(\beta_1)$ is the prior p.d.f. for β_1. We adopt a flat prior, $\pi(\beta_1) = H(\beta_1)$, in this analysis, with H being the Heaviside step function.

The most probable value (MPV) corresponds to the most likely combined single top production cross section given the data. The uncertainty corresponds to the range of highest posterior probability density which covers 68.27%. Performing the likelihood fit with all systematic rate and shape uncertainties included in the likelihood function, we determine a most probable value for the single top cross section of $2.7^{+1.5}_{-1.3}$ pb. The posterior probability density is shown in Figure 5 (a). Figure 5 (b) shows the best fit of the signal and background EPD templates to the CDF II data.

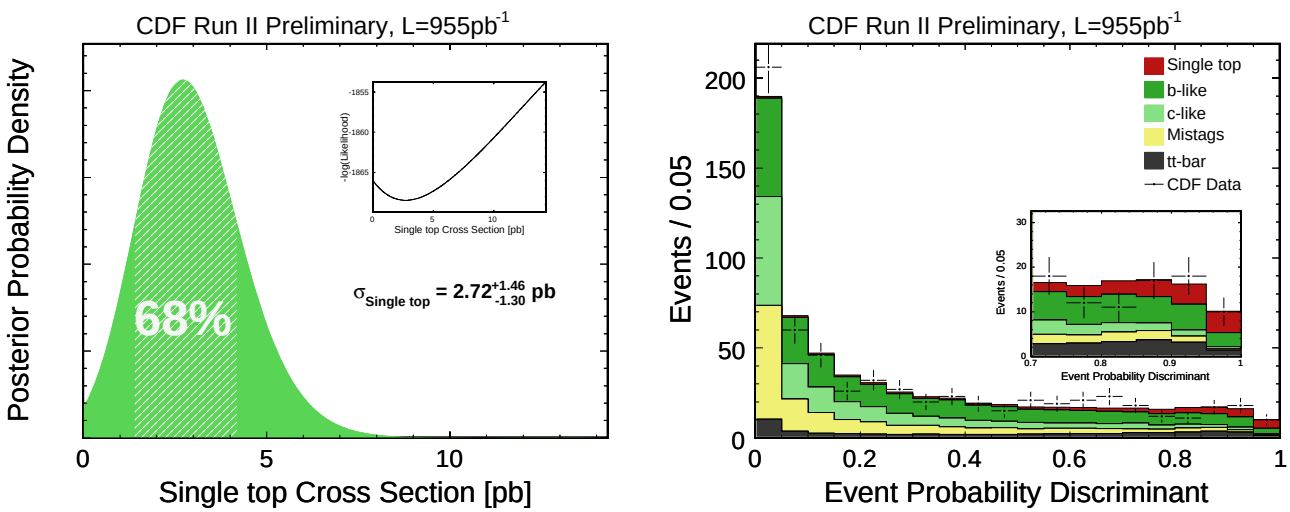

FIG. 5: (a) Cross section result using 955 pb^{-1} of data. The error band shows the 68% uncertainty (all systematics included) on the measurement. (b) Distribution of the event probability discriminant (EPD) for data (644 events) normalized to the best fit of the likelihood method. The insert shows a zoom in the signal region, EPD>0.7

We interprete the result using the CLs/CLb method developed at LEP [7]. We compare our data against two models, one asserting that the data is due to background processes only (H0) and one which includes Standard Model single top production in addition to the background processes (H1). We propagate all systematic uncertainties in our statistical method as described in the previous section . Using the test statistic $Q = -2\ln\frac{P(data)|H1}{P(data)|H0}$ we compute the probability (p-value) that the background only (H0) model fluctuated equal or up to the observed value Q_{obs} in the data (observed p value) and to the median Q value of signal+background (H1) pseudo-experiments (expected p-value). We expect a p-value of 0.6% (2.5σ) and observe a p-value of 1% (2.3σ) in the data.

CONCLUSIONS

We have used the Matrix Element analysis technique for the first time in a direct search for electroweak single top quark production. Our search was done simultaneously for s-channel and t-channel single top production. To extract the most probable single top content in data, we apply a maximum likelihood technique. All sources of systematic rate and shape uncertainty are included in the likelihood function. We have analyzed 955 $pb^{-1}$of CDF Run II data

and measure a combined s- and t-channel single top production cross section of:

$$\sigma_{singletop} = 2.7^{+1.5}_{-1.3} \text{ pb (all systematics included)}$$

assuming a top quark mass of 175 GeV/c^2. We use the CLs/CLb method to calculate the signal significance. The observed p-value in $955pb^{-1}$ of CDF data is 1.0%. The expected (median) p-value in pseudo-experiments is 0.6%.

We thank the Fermilab staff and the technical staffs of the participating institutions for their vital contributions. This work was supported by the U.S. Department of Energy and National Science Foundation; the Italian Istituto Nazionale di Fisica Nucleare; the Ministry of Education, Culture, Sports, Science and Technology of Japan; the Natural Sciences and Engineering Research Council of Canada; the National Science Council of the Republic of China; the Swiss National Science Foundation; the A.P. Sloan Foundation; the Bundesministerium fuer Bildung und Forschung, Germany; the Korean Science and Engineering Foundation and the Korean Research Foundation; the Particle Physics and Astronomy Research Council and the Royal Society, UK; the Russian Foundation for Basic Research; the Comision Interministerial de Ciencia y Tecnologia, Spain; and in part by the European Community's Human Potential Programme under contract HPRN-CT-20002, Probe for New Physics.

[1] see for example T. M.P. Tait, C.-P. Yuan, "Single Top Production as a Window to Physics Beyond the Standard Model", Phys. Rev. D **63**, 014018 (2000).
`http://arxiv.org/abs/hep-ph/0007298` and references therein.

[2] Z.Sullivan, Phys. Rev. D **70**, 114012 (2004).

[3] D0 Collaboration, V.M. Abazov, et, al., Nature 429 (2004); D0 Collaboration, V.M. Abazov, et. al., Phys. Lett. **B** 617 (2005); F. Canelli, PhD thesis, University of Rochester (2003); `ttp://www-cdf.fnal.gov/`pysics/new/top/2006/mass/ljets_meat_1fb/index.html.

[4] B. Stelzer, PhD Thesis, University of Toronto, FERMILAB-THESIS-2005-79.
`http://www.slac.stanford.edu/spires/find/hep/www?r=umi-nr07812`

[5] L. Demortier, *Bayesian treatments of Systematic Uncertainties*, Proceedings of Advanced Statistical Techniques in Particle Physics, Grey College, Durham, 18 - 22 March 2002,
http://www.ippp.dur.ac.uk/Workshops/02/statistics/proceedings.shtml

[6] C. Ciobanu, T. Junk, T. Müller, P. Savard, B. Stelzer, W. Wagner, T. Walter, *Likelihood Function for Single Top Search with 162 pb^{-1}*, CDF Note 7106 (2004)

[7] L. Read, J.Phys G **28**, 2693 (2002) and T. Junk, Nucl. Instum. Meth. **434**, 435 (1999). See also P. Bock *et al.* (The LEP Collaborations), CERN-EP-98-046 (1998) and CERN-EP-2000-055 (2000).